Electronic Supplementary Information

Construction of robust Cu-MOFs from bifunctional pyridine-hydroxamate linkers for photocatalytic CO_2 reduction

Li Xiong,[a] Wenlei Tang,[a] Chaozhi Xiong,[a] Jiajun Du,[a] Zhiyuan Zhang,[a] Yuqing Qiu,[a] Zhen-Wu Shao,[a]* Xuemei Zhou[a]* and Chong Liu[a]*

Contents

1.General procedures

1.1 Materials and reagents

Methyl isonicotinate (98%), hydroxylamine hydrochloride (99%), sodium hydroxide (≥96.0%), ammonium hydroxide (25-28%), Copper(II) Nitrate Hemi(Pentahydrate) (98.0%), Nafion (5 wt.% in mixture of lower aliphatic alcohols and water, contains 45% water), Na_2SO_4 (≥99.0%), EtOH (≥99.7%), $NaHCO_3$ (≥99.0%), N,N-dimethylformamide (99.8%) were purchased from Adamas and used as received. Ultrapure water was obtained from a Millipak Express 40 system (Merk-Millipore, Darmstadt, Germany).

1.2 Characterization

Optical images were acquired with a Rui Hong BM-500T optical microscope.

^{1}H NMR spectrum was collected on a JNM-ECZ400S/L1 (400 MHz) spectrometer (JEOL Ltd., Tokyo, Japan).

Powder X-ray diffraction (PXRD) patterns were collected using a Rigaku MiniFlex600 operating at 40 kV, 40 mA for Cu Kα, (λ = 1.54178 Å) with a scan speed of 10°/min from 3 to 50° at a step size of 0.01°.

Single-crystal XRD data were collected on Bruker D8 Venture single crystal X-ray diffractometers (Mo Kα radiation, λ = 0.71073 Å, CuKα radiation, λ = 1.54178, GaKα radiation, λ = 1.34139). The data were collected and integrated to 0.78 Å (SUM-23A/B) and 0.77 Å (SUM-33), and empirical absorption correction was applied. The structure was solved with direct method using SHELXT[1] and refined by full-matrix least-squares on F^2 using SHELXL[2] in Olex2.[3] All non-H atoms were located easily and refined anisotropically. Idealized atom positions were calculated for H atoms.

Thermogravimetric analysis (TGA) was carried out on a TA Discovery SDT 650 simultaneous thermal analyzer from room temperature to 800 °C at a heating rate of 10 °C/min in a N_2 flow of 100 mL/min.

UV-vis diffuse reflectance spectra were collected on a Shimadzu UV-3600 using an integrating-sphere accessory. The measured wavelength range was 200–800 nm. $BaSO_4$ powder was used as a reference standard.

The photoluminescence (PL) spectra were recorded on an Edinburgh FLS1000 spectrophotometer with an excitation wavelength of 363 nm. The emission ranging 400–700 nm

at room temperature was acquired. The samples were pressed into a pellet on quartz before measurement. The PL spectrum for each sample was an average of three measurements. The fluorescence decay profiles were also recorded using the FLS1000 at the excitation wavelength of 363 nm.

X-ray photoelectron spectroscopy (XPS) was performed using a Thermo Scientific K-Alpha to obtain the chemical composition of the surface and the corresponding elemental valence states of the MOF samples, using full and fine spectrum X-ray electron scanning.

Photoelectrochemical measurements were carried out on an Autolab PGSTAT204A electrochemical workstation, details are given in Section 4.

Photocatalytic performance was performed in a 250 mL Pyrex glass reactor (Labsolar 6A, Beijing Perfect Light). The reactor was illuminated by a 300 W Xe lamp and an AM1.5 solar simulator. The temperature was maintained at 25 °C during the reaction using a circulating water-cooling system. The gaseous products were analyzed by a gas chromatograph (GC-14C, Shimadzu, Japan) with a blocked discharge ionization detector (BID), using high purity helium (99.999%) as carrier gas and Carboxen@1010 PLOT (30 mm × 0.53 mm) as column. The liquid solution was also analyzed in GC.

Scanning electron microscopy (SEM) images were obtained using a JEOL JSM-7610 at an accelerating voltage of 15 kV.

2. Syntheses of 4-PyHA, SUM-23A, SUM-23B and SUM-33

2.1 Synthesis of 4-pyridinehydroxamic acid

The synthesis of ligand 4-pyridinehydroxamic acid (4-PyHA) was carried out according to the procedure previously reported.[4] The identity and purity of the ligand were confirmed by ^{1}H NMR (Fig. S1).

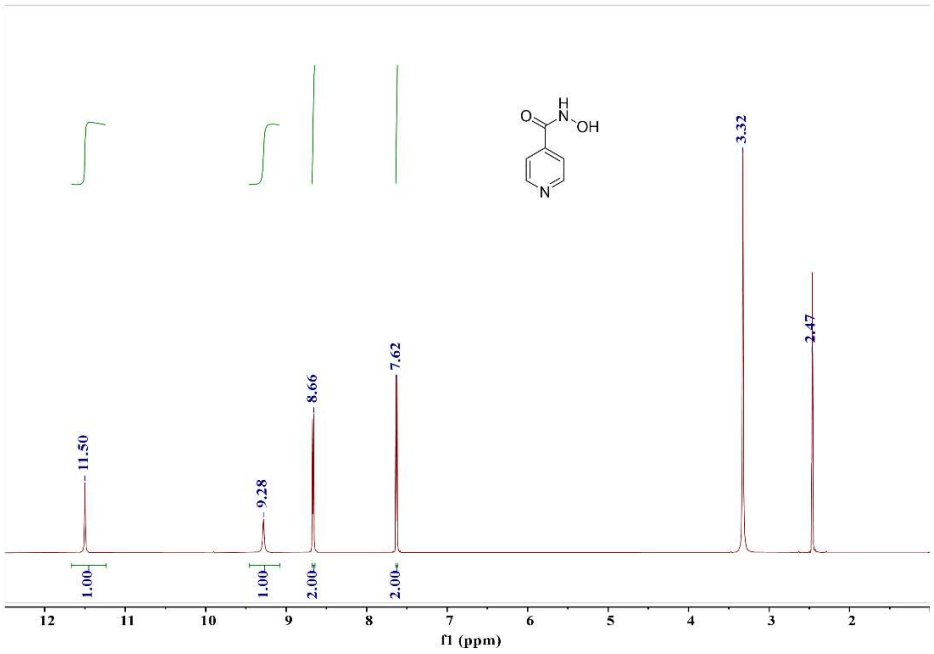

Fig. S1 ^{1}H NMR spectrum of 4-PyHA in DMSO-d_6.

2.2 Synthesis of SUM-23A

4-PyHA (2.1 mg, 0.015 mmol) and $Cu(NO_3)_2 \cdot 2.5H_2O$ (9.3 mg, 0.04 mmol) were dissolved in DMF (1.0 mL) by ultrasonication, and then sealed in a 4-mL glass vial. The mixture was heated in an isothermal oven at 100 ℃ for 1 day. Octahedral crystals were collected by centrifugation (Fig. S2) and washed with fresh DMF. The crystal structure was determined by single crystal X-ray crystallography and named SUM-23A.

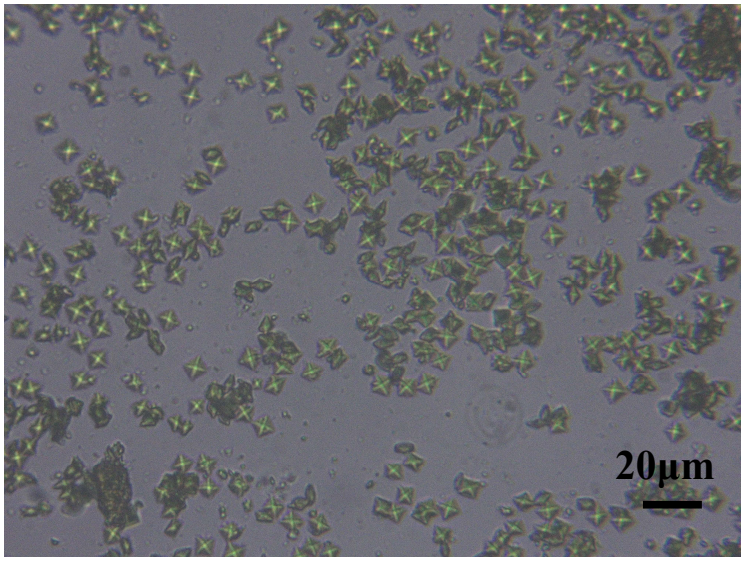

Fig. S2 Optical image of SUM-23A crystals.

2.3 Synthesis of SUM-23B

SUM-23A crystals, synthesized as described in Section 2.2, were washed with fresh EtOH (3×) to facilitate the transformation to a new phase. The crystal structure was determined by single crystal X-ray crystallography and named SUM-23B.

2.4 Synthesis of SUM-33

4-PyHA (16.6 mg, 0.12 mmol) and $Cu(NO_3)_2 \cdot 2.5H_2O$ (7 mg, 0.03 mmol) were dissolved in a mixture of DMF (1.0 mL) and $NH_3 \cdot H_2O$ (0.2 mL) by ultrasonication, and then sealed in a 4-mL glass vial. The mixture was heated in an isothermal oven at 100 ℃ for 1 day. Rod-shaped crystals were collected by centrifugation (Fig. S3) and washed with fresh DMF. The crystal structure was determined by single crystal X-ray crystallography and named SUM-33.

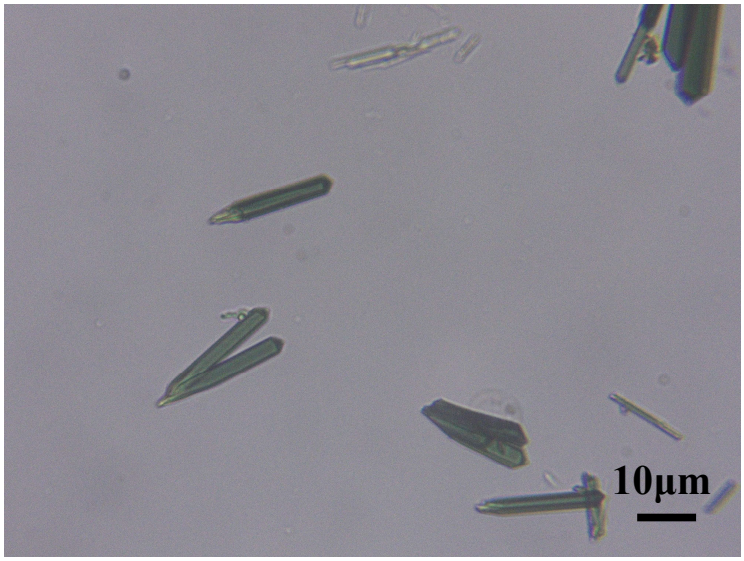

Fig. S3 Optical image of SUM-33 crystals.

3. Crystal structures of SUM-23A, SUM-23B and SUM-33

3.1 Crystal structure of SUM-23A

Table S1 Crystal data and structure refinement details for SUM-23A.

CCDC deposition number	2410552
Compound name	SUM-23A
Formula	$C_{48}H_{44}Cu_{10}N_{16}O_{22}$
Formula weight	1832.39
Temperature/K	193.0
Crystal system	tetragonal
Space group	*I*-4*c*2
a/Å	23.1107(2)
b/Å	23.1107(2)
c/Å	18.0067(4)
α/°	90
β/°	90
γ/°	90
Volume/Å^3	9617.5(3)
Z	4
ρ_{calc} g/cm^3	1.266
μ/mm-1	2.849
F(000)	3640.0
Crystal size/mm^3	0.13 × 0.12 × 0.1
Radiation	CuKα (λ = 1.54178)
Theta range for data collection /°	5.408 to 160.02
Index ranges	$-29 \leq h \leq 28$, $-29 \leq k \leq 29$, $-22 \leq l \leq 21$
Reflections collected	74193
Independent reflections	5155 [R_{int} = 0.0381, R_{sigma} = 0.0148]
Data / restraints / parameters	5155/32/240
Goodness-of-fit on F^2	1.098
Final R indexes [I>=2σ (I)]	R_1 = 0.0338, wR_2 = 0.0922
R indices (all data)	R_1 = 0.0351, wR_2 = 0.0930
Largest diff. peak and hole /e Å^{-3}	0.73/-0.35

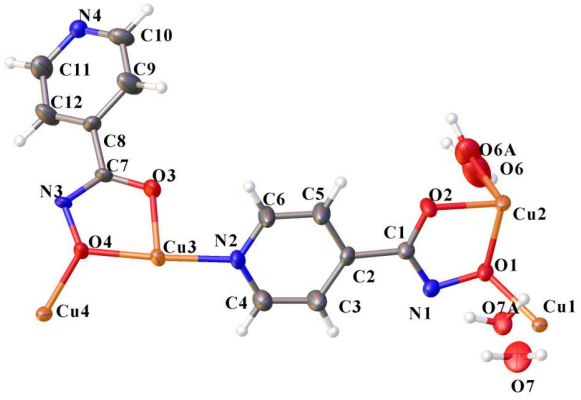

Fig. S4 ORTEP diagram of the asymmetric unit of SUM-23A (50% probability factor for the thermal ellipsoids), generated via Olex2-1.5.

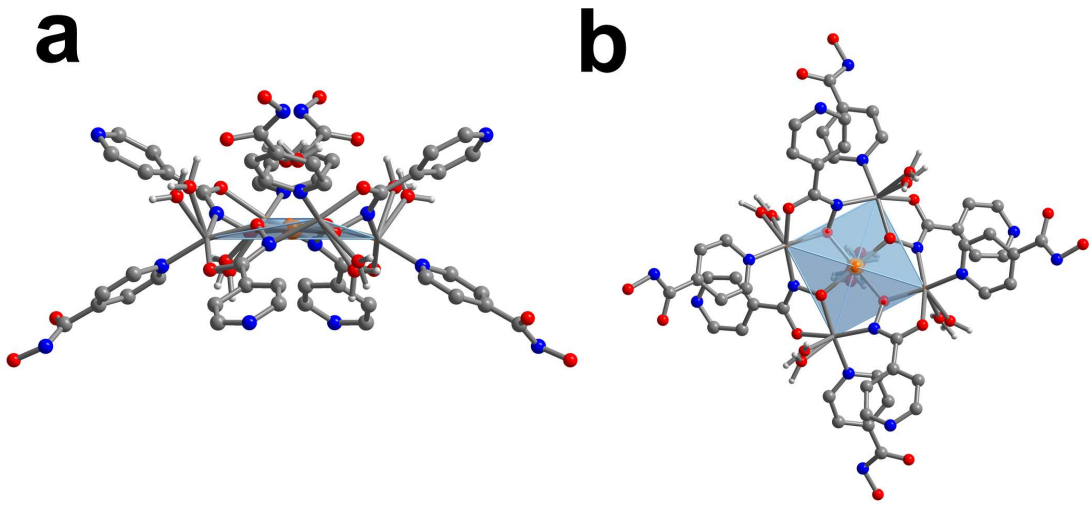

Fig. S5 Coordination environment of Cu atoms in SUM-23A is observed from the *x* (left) and y (right) directions. Color codes: Cu, orange spheres; C, light grey spheres; N, light blue spheres; O, red spheres; H, omitted for clarity.

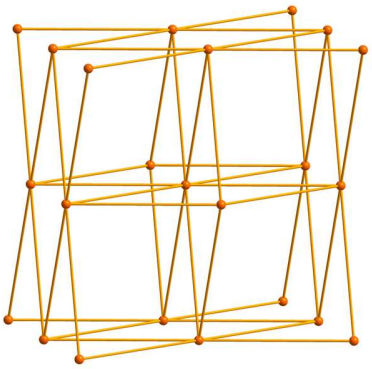

Fig. S6 Body-centered cubic (**bcu**) topology of SUM-23A.

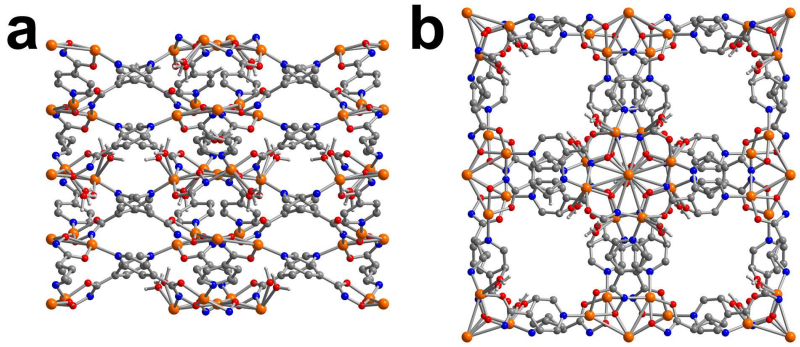

Fig. S7 Crystal structure of SUM-23A, observed in the *y*(a) and *z*(b) directions. Cu: orange spheres; C: light grey spheres; N: light blue spheres; O: red spheres; H: omitted for clarity.

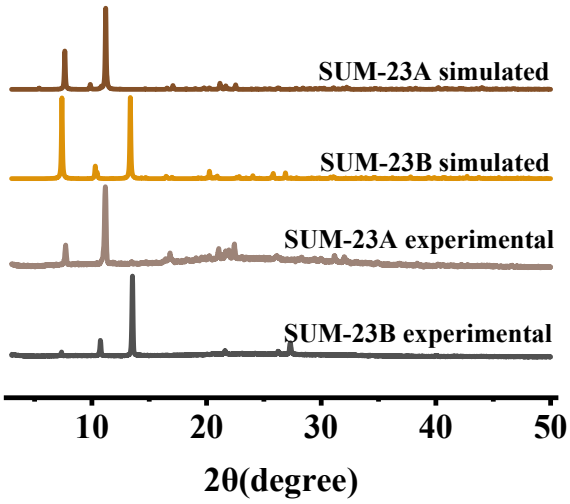

Fig. S8 PXRD patterns of SUM-23A and SUM-23B, comparing the experimental with the simulated from SC-XRD structures.

3.2 Crystal structure of SUM-23B

Table S2 Crystal data and structure refinement details for SUM-23B.

CCDC deposition number	2410553
Compound name	SUM-23B
Formula	$C_{24}H_{16}Cu_5N_8O_8$
Formula weight	862.15
Temperature/K	193.0
Crystal system	tetragonal
Space group	*I*-4*c*2
a/Å	23.9056(8)
b/Å	23.9056(8)
c/Å	14.4066(10)
α/°	90
β/°	90
γ/°	90
Volume/Å^3	8233.1(8)
Z	8
ρ_{calc} g/cm^3	1.391
μ/mm-1	14.002
F(000)	3400.0
Crystal size/mm^3	0.13 × 0.12 × 0.1
Radiation	GaKα (λ = 1.34139)
Theta range for data collection /°	4.548 to 107.796
Index ranges	$-28 \leq h \leq 26$, $-28 \leq k \leq 27$, $-17 \leq l \leq 17$
Reflections collected	16571
Independent reflections	3653 [R_{int} = 0.1208, R_{sigma} = 0.1140]
Data / restraints / parameters	3653/0/204
Goodness-of-fit on F^2	0.991
Final R indexes [I>=2σ (I)]	R_1 = 0.0803, wR_2 = 0.2011
R indices (all data)	R_1 = 0.1483, wR_2 = 0.2425
Largest diff. peak and hole /e Å^{-3}	0.54/-0.67

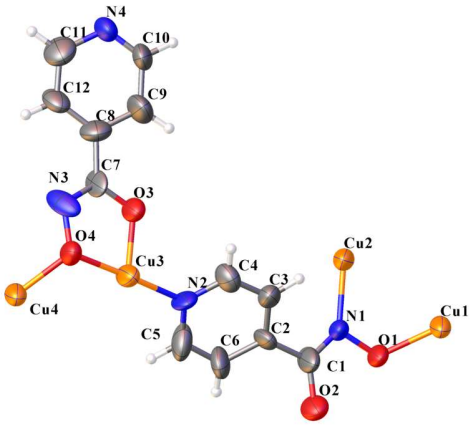

Fig. S9 ORTEP diagram of the asymmetric unit of SUM-23B (50% probability factor for the thermal ellipsoids), generated via Olex2-1.5.

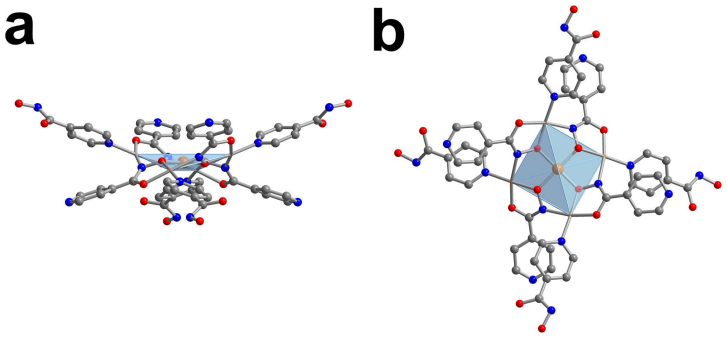

Fig. S10 Coordination environment of Cu in SUM-23B is observed from the *y* (left) and *z* (right) directions. Color codes: Cu, orange spheres; C, light grey spheres; N, light blue spheres; O, red spheres; H, omitted for clarity.

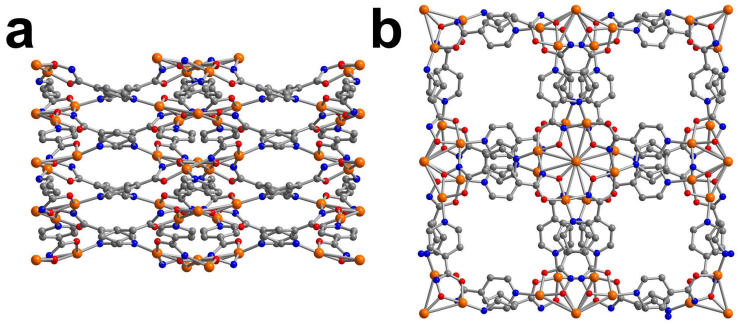

Fig. S11 Crystal structure of SUM-23B, observed in the *y* (left) and *z* (right) directions. Color codes: Cu, orange spheres; C, light grey spheres; N, light blue spheres; O, red spheres; H, omitted for clarity.

3.3 Crystal structure of SUM-33

Table S3 Crystal data and structure refinement details for SUM-33.

CCDC deposition number	2410554
Compound name	SUM-33
Formula	$C_6H_4CuN_2O_2$
Formula weight	199.65
Temperature/K	223.00
Crystal system	orthorhombic
Space group	*Pna*2$_1$
a/Å	11.5203(4)
b/Å	15.0467(5)
c/Å	4.4357(2)
α/°	90
β/°	90
γ/°	90
Volume/Å^3	768.90(5)
Z	4
ρ_{calc} g/cm^3	1.725
μ/mm-1	2.786
F(000)	396.0
Crystal size/mm^3	0.12 × 0.11 × 0.09
Radiation	MoKα (λ = 0.71073)
Theta range for data collection /°	4.452 to 55.07
Index ranges	-14 ≤ h ≤ 14, -19 ≤ k ≤ 19, -5 ≤ l ≤ 5
Reflections collected	24274
Independent reflections	1769 [R_{int} = 0.0561, R_{sigma} = 0.0247]
Data / restraints / parameters	1769/1/100
Goodness-of-fit on F^2	1.126
Final R indexes [I>=2σ (I)]	R_1 = 0.0209, wR_2 = 0.0557
R indices (all data)	R_1 = 0.0228, wR_2 = 0.0568
Largest diff. peak and hole /e Å^{-3}	0.23/-0.42

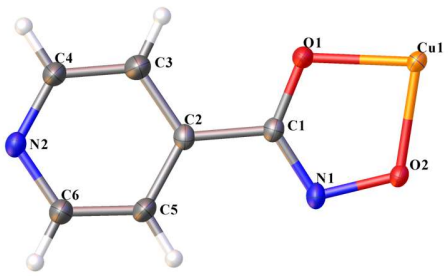

Fig. S12 ORTEP diagram of the asymmetric unit of SUM-33 (50% probability factor for the thermal ellipsoids), generated via Olex2-1.5.

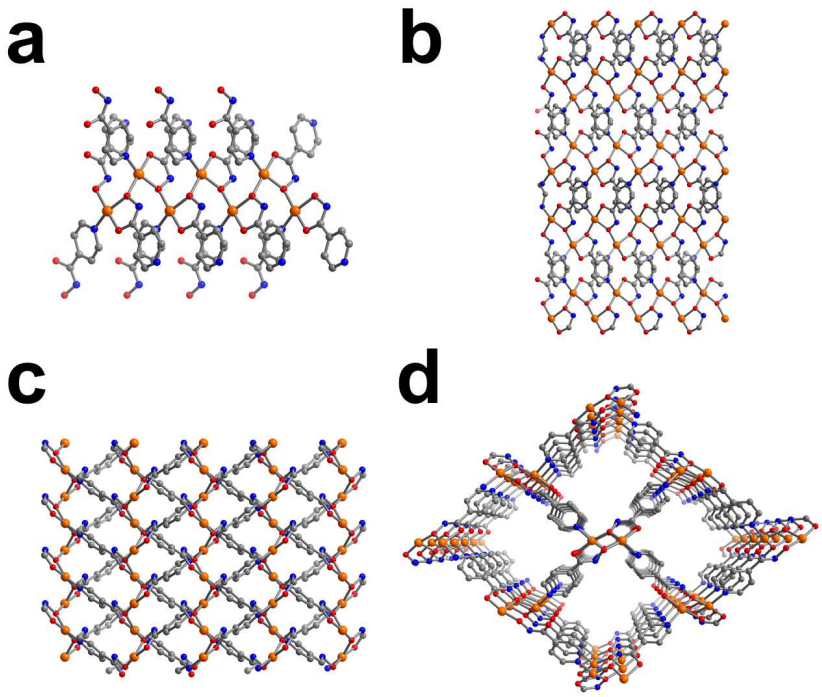

Fig. S13 (a) Coordination environment of Cu in SUM-33; (b)(c)(d) The crystal structure as viewed in the *x*, *y*, and *z* directions, respectively. Color codes: Cu, orange spheres; C, light grey spheres; N, light blue spheres; O, red spheres; H, omitted for clarity.

4. Characterization of SUM-23A, SUM-23B and SUM-33

4.1 X-ray photoelectron spectroscopy (XPS) of SUM-23B

The oxidation states of Cu in SUM-23B were revealed by XPS: Cu^{2+}: Cu^{1+} = 3:2.

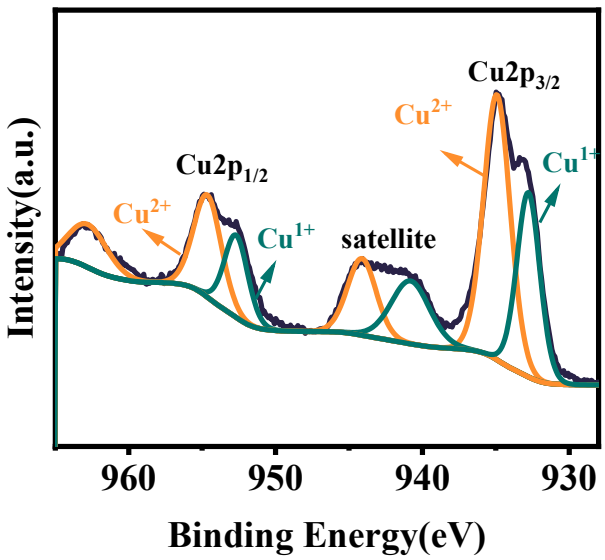

Fig. S14 Cu2p XPS spectrum of newly synthesised SUM-23B.

4.2 Crystallinity test of SUM-23 and SUM-33 in various media

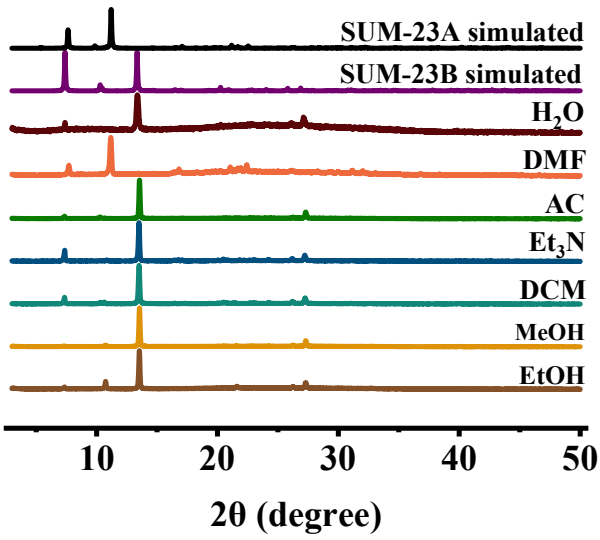

Fig. S15 PXRD patterns of SUM-23, comparing the simulated to the experimental after soaking in corresponding solvents for 24 h.

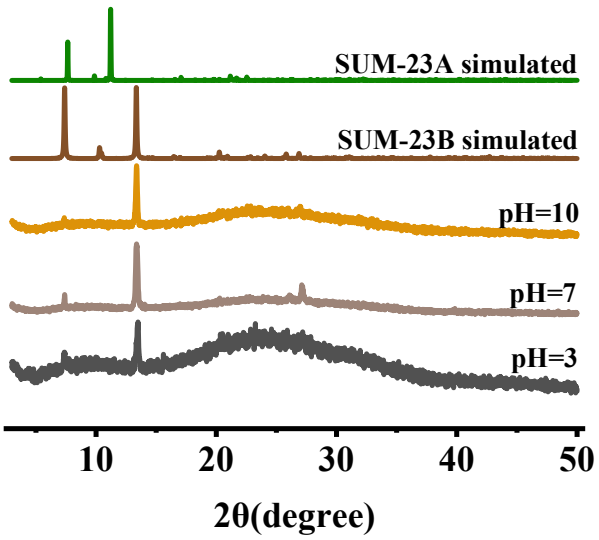

Fig. S16 PXRD patterns of SUM-23 after exposure to aqueous solutions of different pH for 24 h, compared with the simulated patterns.

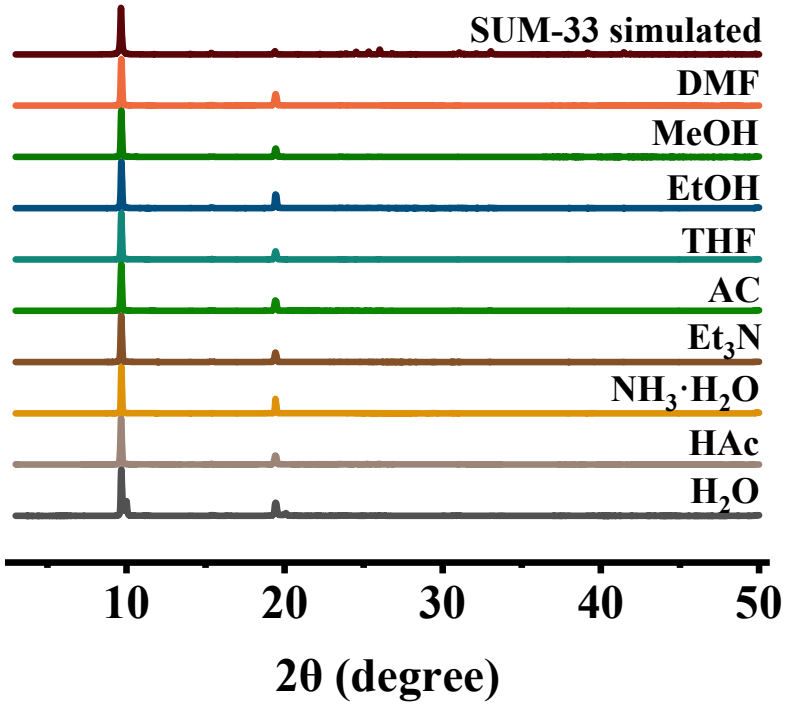

Fig. S17 PXRD patterns of SUM-33, comparing the simulated to the experimental after soaking in corresponding solvents for 24 h.

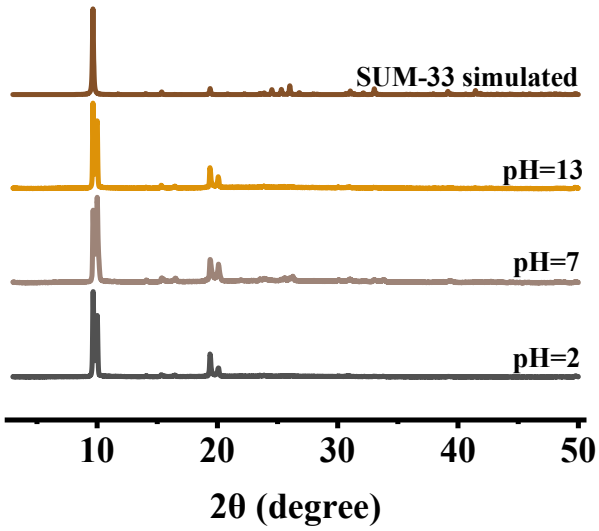

Fig. S18 PXRD patterns of SUM-33 after exposure to aqueous solutions of different pH for 24 h, compared with the simulated pattern.

4.3 Gas sorption of SUM-23B and SUM-33

The same activation procedure was performed for SUM-23B and SUM-33: the as-synthesized MOFs were washed with dry DMF (3×) and exchanged with acetone (3×) for 72 h, followed by activation at 100 ºC for 12 h on a degassing station of BELSORP MAX. The N_2 adsorption data (Fig. 1e of the main text) obtained at 77 K were fitted to the specific surface area (Fig. S19-S20, Table S4-S5). Non-local density functional theory (NLDFT) was applied to the adsorption data points using the cylindrical pore metal oxide model to estimate the pore size distribution, as shown in Fig. S21-S22. Using the activated samples described above, CO_2 adsorption data were obtained at 273.15 K, 293.15 K, 298.15 K, 303.15 K and 308.15 K (Fig. S23-S24).

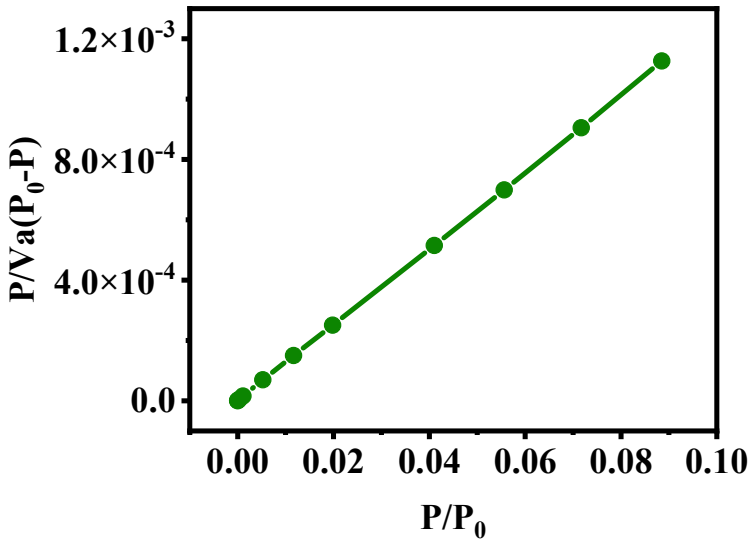

Fig. S19 Specific surface area fitting curve for SUM-23B.

Table S4 Parameters for SUM-23B calculated from BET analysis.

SUM-23B	
BET Area(m^2g^{-1})	344.19
Slope	1.26×10^{-2}
Intercept	4.13×10^{-7}
R^2	0.99632
C	30646
Vm[cm^3(STP)g^{-1}]	79.078

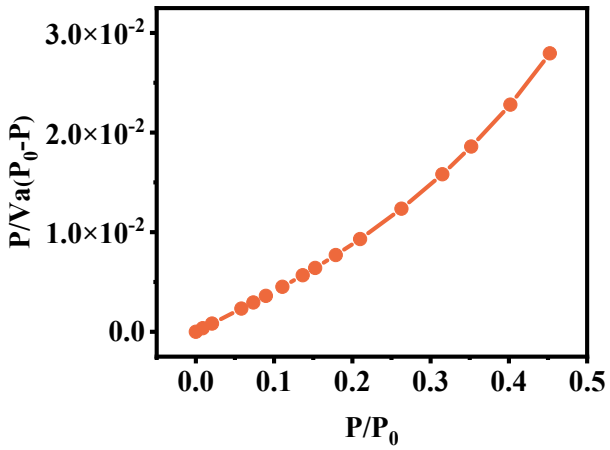

Fig. S20 Specific surface area fitting curve for SUM-33.

Table S5 Parameters for SUM-33 calculated from BET analysis.

SUM-33	
BET Area(m^2g^{-1})	110.59
Slope	3.94×10^{-2}
Intercept	9.25×10^{-7}
R^2	1
C	42554
Vm[cm^3(STP)g^{-1}]	25.408

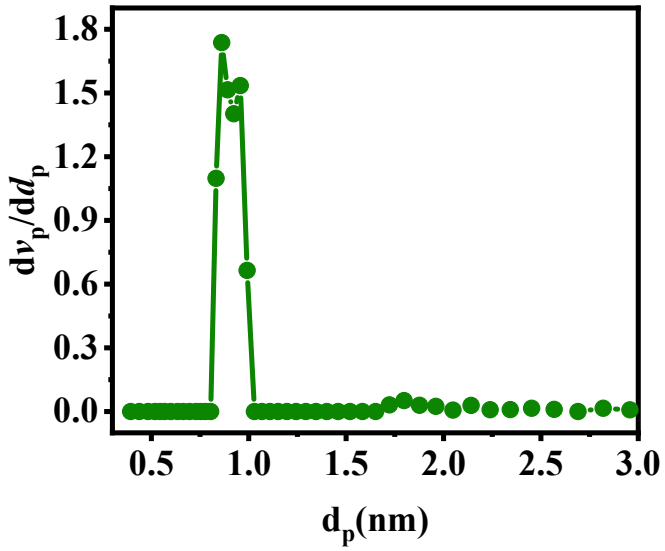

Fig. S21 SUM-23B pore size distribution.

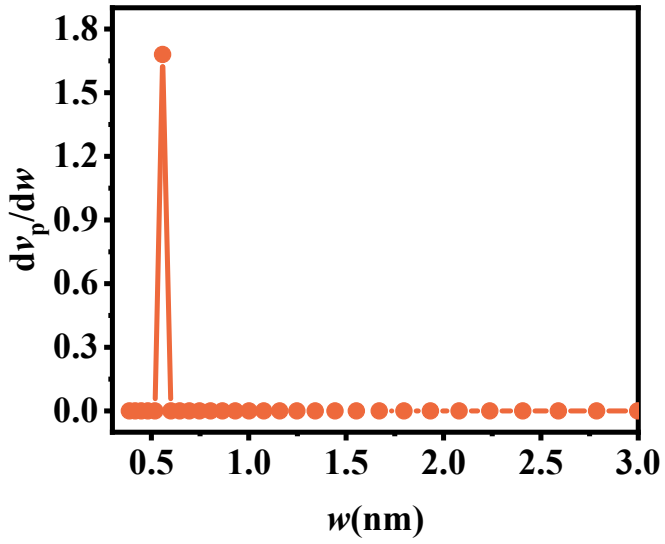

Fig. S22 SUM-33 pore size distribution.

The CO_2 uptake capacity was calculated using the following equation:

$$\ln(p) = \ln(N) + \left(\frac{1}{T}\right)\sum_{i=0}^{m} a_i \times N^i + \sum_{j=0}^{n} b_j \times N^j$$

Where N (mg/g) is the adsorption capacity, p (mmHg) is the pressure, T (K) is the temperature, a_i and b_i are empirical constants.

The isosteric heat of adsorption (Q_{st}) was calculated using the following equation (Fig. S25-S26):

$$Q_{st} = -R \times \sum_{i=0}^{m} a_i \times N^i$$

Where R is the universal gas constant (8.314 $Jmol^{-1}K^{-1}$).

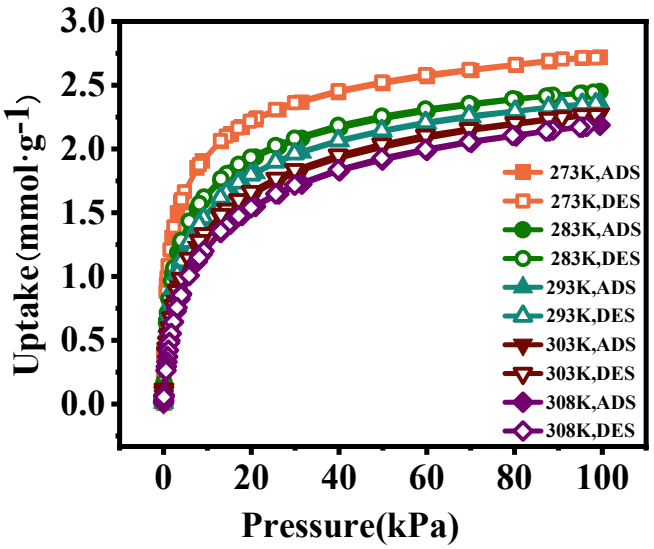

Fig. S23 SUM-23B CO_2 adsorption–desorption isotherms.

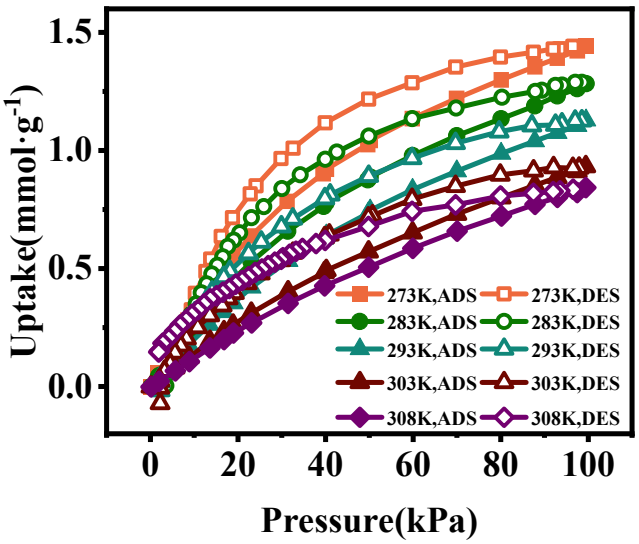

Fig. S24 SUM-33 CO_2 adsorption–desorption isotherms.

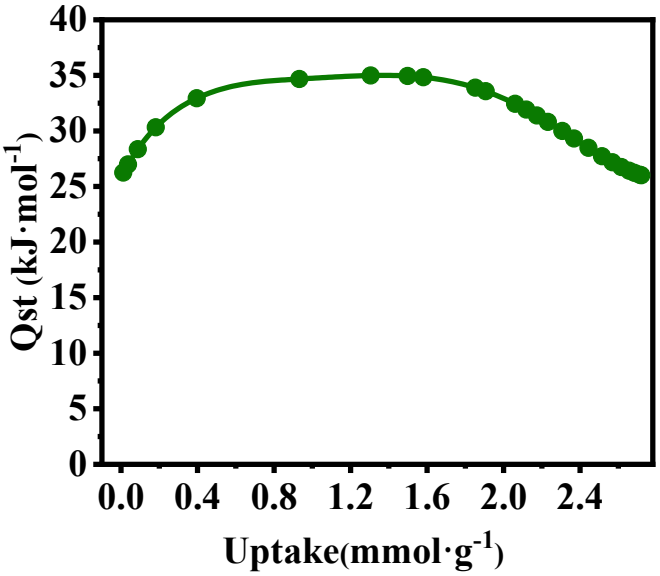

Fig. S25 Q_{st} toward CO_2 for SUM-23B.

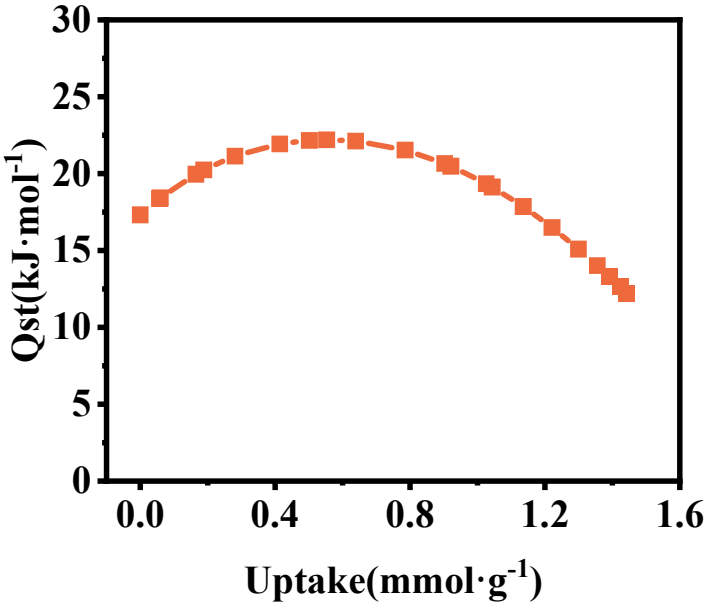

Fig. S26 Q_{st} toward CO_2 for SUM-33.

Table S6 Comparison of CO_2 adsorption capacity of different MOFs.

MOF	Pressure(bar)	Temperature (K)	Capacity (mmol·g^{-1})	Ref.
MOF-2	35	298	3.2	[5]
SNU-5	1	273	0.9	[6]
Cu-BTTri	1	298	3.2	[7]
Fe-BTT	1	298	3.1	[8]
$[Cd_2L1(H_2O)]_2$	1	293	2.1	[9]
TMOF-1	1	273	2.2	[10]
PCN-123	1	295	1	[11]
ZIF-100	1	273	1.7	[12]
$Zn_3(OH)(pcdc)_{2.5}$	0.5	298	0.568	[13]
HKUST-1	1	273	7.23	[14]
SUM-1	1	273	3.2	[15]
SUM-9	1	273	1.4	[15]
SUM-23B	1	273	2.7	**This work**
SUM-33	1	273	1.4	**This work**

4.4 Time-resolved photoluminescence of SUM-23B and SUM-33

The fluorescence lifetimes of SUM-23B and SUM-33 were determined using the following equations. The fluorescence lifetimes of SUM-23B and SUM-33 were determined based on a

single-exponential fit to the fluorescence decay graph (Fig. 3b in the main text) using the following equations.

$$y(t) = A_1 e^{(-\frac{t}{\tau_1})} + y_0$$

Table S7 Parameters of the single-exponential fit of the PL decay curves

Name	τ_1(ns)	Std.dev.(ns)	R^2
SUM-23B	0.61	-	0.97731
SUM-33	0.74	0.00528	0.98137

4.5 Electrochemical characterization of SUM-23B and SUM-33

A Pt sheet served as the counter electrode, a saturated Ag/AgCl electrode was used as the reference, and MOF samples were the working electrodes. Na_2SO4 solution (0.1 M) with pH = 7.03 was used as the electrolyte.The working electrode was prepared by ultrasonicating 5.0 mg of MOF photocatalyst in 1 mL of ethanol and 0.02 mL of 5 wt.% Nafion solution for about 15 minutes for uniform suspensions. 50 μL(×10) of the suspension was spin coated on the surface of an FTO plate (1.5 × 1.0 cm^2).

4.6 DFT calculation:

DFT calculations were performed using the Gaussian16 software package. The ground state was calculated at the B3LYP/genecp (Cu: LanL2dz, C/H/O/N: 6-31G) level.

Table S8 Cartesian Coordinates of the SUM-33 structural unit for DFT/B3LYP Optimization

atom	x	y	z
N	4.5315	4.934	2.8566
C	3.5898	5.3332	3.7116
C	4.5637	3.6296	2.5472
C	2.6615	4.4825	4.2697
H	3.5573	6.243	3.9456
C	2.6747	3.1396	3.9251
H	2.0243	4.8092	4.8789
C	1.7091	2.2126	4.5665
C	3.6526	2.7232	3.0504
O	1.022	2.6826	5.5664
N	1.6548	0.99	4.1258
H	3.7016	1.8193	2.7962
Cu	-0.0189	1.3084	6.3594

O	0.7701	0.2458	4.9684
H	5.2322	3.3198	1.9638
N	-1.2285	2.5902	7.2921
C	-2.1708	2.1904	8.1474
C	-1.197	3.894	6.983
C	-3.0985	3.0405	8.7055
H	-2.2026	1.28	8.3814
C	-2.107	4.8001	7.4861
H	-0.5278	4.2032	6.3996
C	-3.0853	4.3838	8.3609
H	-3.7357	2.7142	9.3147
H	-2.0587	5.7045	7.2319
C	-4.1217	5.3688	8.9329
O	-3.687	6.5469	9.617
N	-5.558	5.098	8.7756
O	-5.9715	3.9776	8.125
H	-5.2065	3.476	7.8337
H	-6.231	5.7376	9.1471

Table S9 Cartesian Coordinates of the SUM-23 structural unit for DFT/B3LYP Optimization

atom	x	y	z
Cu	23.9056	11.9528	3.6016
Cu	21.0639	13.3769	3.0628
Cu	25.3303	14.7957	4.1409
Cu	26.7485	10.5294	3.0629
Cu	22.4822	9.1111	4.1409
O	22.3406	10.9131	3.5008
O	22.8659	13.519	3.703
O	25.4718	12.9937	3.5008
O	24.9465	10.3878	3.703
N	21.139	11.5259	3.7745
O	21.4104	15.1503	2.4546
N	23.4779	14.719	3.4281
O	27.1022	14.4476	4.7479
N	26.6718	12.3801	3.7745
O	26.4004	8.7557	2.4547
N	24.3329	9.1862	3.4281
O	20.7085	9.4576	4.7479
C	20.3867	10.7313	4.5951
C	22.6848	15.4719	2.6079
C	27.4253	13.1745	4.5951
C	25.1273	8.4339	2.6079
C	19.0858	11.2455	5.0139
C	23.1975	16.7725	2.1896

C	28.7245	12.66	5.014
C	24.6128	7.133	2.1896
C	18.9785	12.5141	5.4459
C	17.9659	10.3941	4.9702
C	24.4675	16.8797	1.7581
C	22.3475	17.8923	2.2338
C	28.8331	11.3912	5.4459
C	29.8457	13.5113	4.9702
C	23.344	7.0257	1.7581
C	25.4641	6.0131	2.2338
H	19.7261	13.1013	5.4171
C	17.7403	12.9612	5.9641
H	18.0103	9.5149	4.6152
C	16.7482	10.9272	5.5174
H	25.0533	16.1318	1.7856
C	24.9132	18.1176	1.2387
H	21.4668	17.8477	2.5875
C	22.8792	19.1098	1.6854
H	28.0838	10.8039	5.4172
C	30.0696	10.9439	5.9641
H	29.7996	14.3903	4.6153
C	31.0617	12.9779	5.5174
H	22.7567	7.7733	1.7856
C	22.8967	5.7875	1.2387
H	26.3431	6.0575	2.5876
C	24.9307	4.7954	1.6854
N	16.6671	12.1812	5.9573

5. Photocatalytic CO_2 reduction

1.28 g of $NaHCO_3$ was dissolved in 50 mL of water and the solution was added to the photocatalytic reactor. 20 mg of the MOF sample was dispersed in 1 mL of deionized water, and the mixture was then deposited on a porous ceramic plate (diameter: 30 mm). The sample was dried at 80 °C for 20 min. After drying, the ceramic plate containing the sample was placed in the center of the reactor. The MOF catalyst was kept above the liquid level in the reactor. After sealing the reactor and vacuuming for 10 min, the pressure stabilized at 0.9 kPa. Then 13 mL of HCl (1 $mol \cdot L^{-1}$) aqueous solution was injected to react with $NaHCO_3$ to generate CO_2 in the reactor, the pressure stabilized at ~45 kPa. During the reaction process, 1 mL of gaseous mixture was extracted from the reactor every hour and analyzed using gas chromatography.

Cyclability test: after reaction, the light was switched off, the reactor was emptied, the catalyst-coated ceramic plate was removed and stored away from light, and the next photocatalytic experiment was operated as described above.

Comparative test: 1.28 g of $NaHCO_3$ was dissolved in 50 mL of water and the solution was added to the photocatalytic reactor. 20 mg of the MOF sample was dispersed in 1 mL of deionized water, and the mixture was then deposited on a porous ceramic plate (diameter: 30 mm). The sample was dried at 80 °C for 20 min. After drying, the ceramic plate containing the sample was placed in the center of the reactor. The MOF catalyst was kept above the liquid level in the reactor. After sealing the reactor and vacuuming for 10 min, the pressure stabilized at 0.9 kPa. Then N_2 was injected to ensure that the system pressure is ~45kpa. During the reaction process, 1 mL of gaseous mixture was extracted from the reactor every hour and analyzed using gas chromatography.

The product yield of gas is calculated by the following equation (for Fig. 3d in the main text):

$$n = V/V_m$$

$$Yield = n/m$$

The productive rates of products (r) are calculated by the following equation:

$$r = n/(mt)$$

where V_m is the molar volume of gas (22.4 L mol^{-1}), n refers to the moles of generated CO (or CH_4), and V is the gas volume, t is the irradiation time, and m is the mass of the photocatalyst.

The selectivity of the generated product based on the required electrons for carbon dioxide reduction is calculated using the following formula:

$$S_{CO} = \frac{2R_{CO}}{2R_{CO} + 8R_{CH_4}} \times 100\%$$

where *R* is the productive rates of products, and the coefficient before *R* represents the number of electrons consumed.

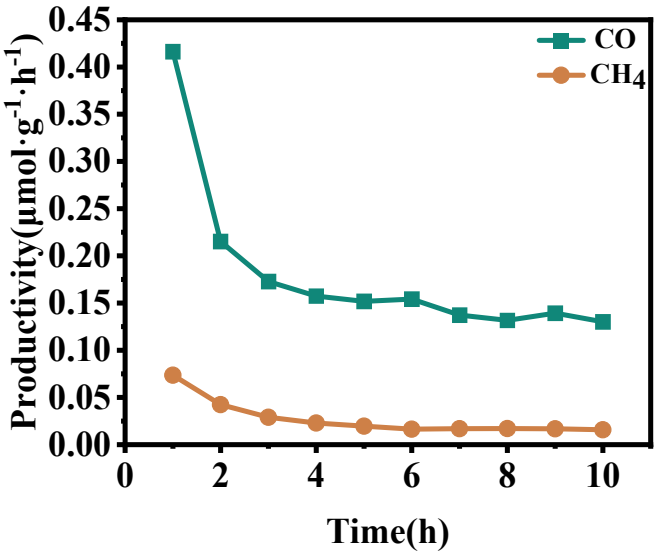

Fig. S27 CO(CH_4) productivity over time under irradiation in the presence of SUM-23B

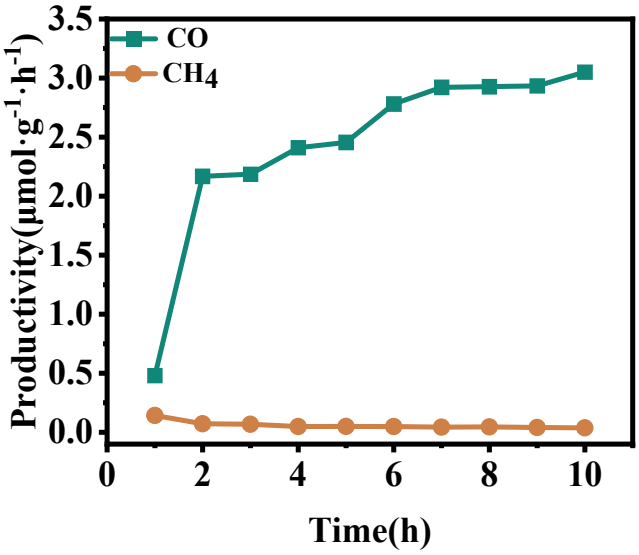

Fig. S28 CO(CH_4) productivity over time under irradiation in the presence of SUM-33

Table S10 Comparison of CO_2 photoreduction activity of different MOFs.

MOF	Main product	Productivity(μmolg^{-1}h^{-1})	Ref.
ZrPP-1-Co	CO	14	[16]
ZrPP-1-Fe	CO	4.1	[16]
ZrPP-1-Cu	CO	2.7	[16]
UiO-66/bulk CN	CO	3.2	[17]
Zn_2GeO_4/Mg-MOF-74	CO	1.4	[18]
Mg-MOF-74	CO	0.06	[18]
NH2-UiO-66	CO	1.6	[19]
UiO-66	CO	0.3	[20]
Cu-TCPP	CO	1	[20]
PCN-224(Cu)	CO	3.7	[21]
MAF-34-CoRu	CO	11.2	[22]
Bulk Zn-MOF-NH_2	CO	3.1	[23]
2D-Zn-MOF-NH_2	CO	18.7	[23]
MIL-101-Cr	CO	8.3	[24]
SUM-23B	CO	0.02	This Work
SUM-33	CO	3.05	This Work

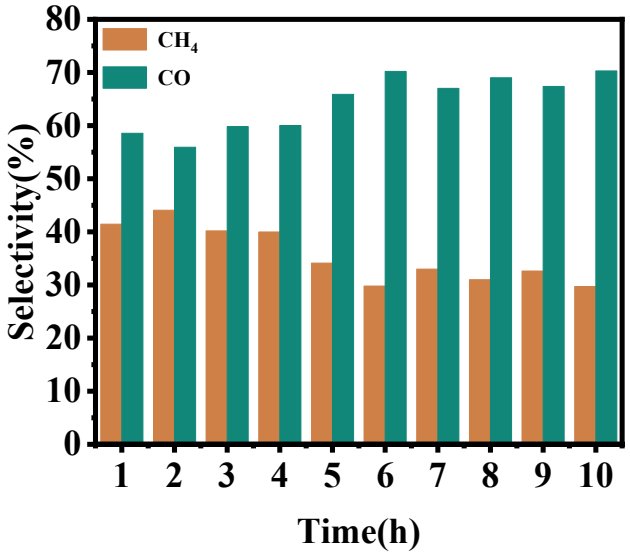

Fig. S29 CO(CH_4) selectivity over time under irradiation in the presence of SUM-23B

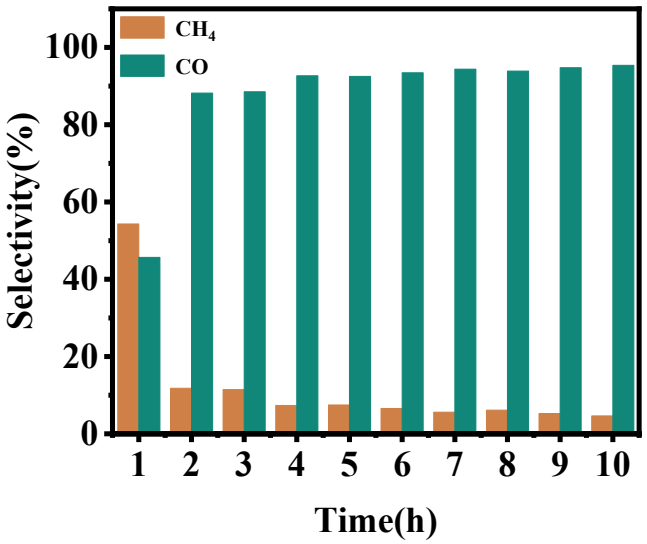

Fig. S30 CO(CH_4) selectivity over time under irradiation in the presence of SUM-33

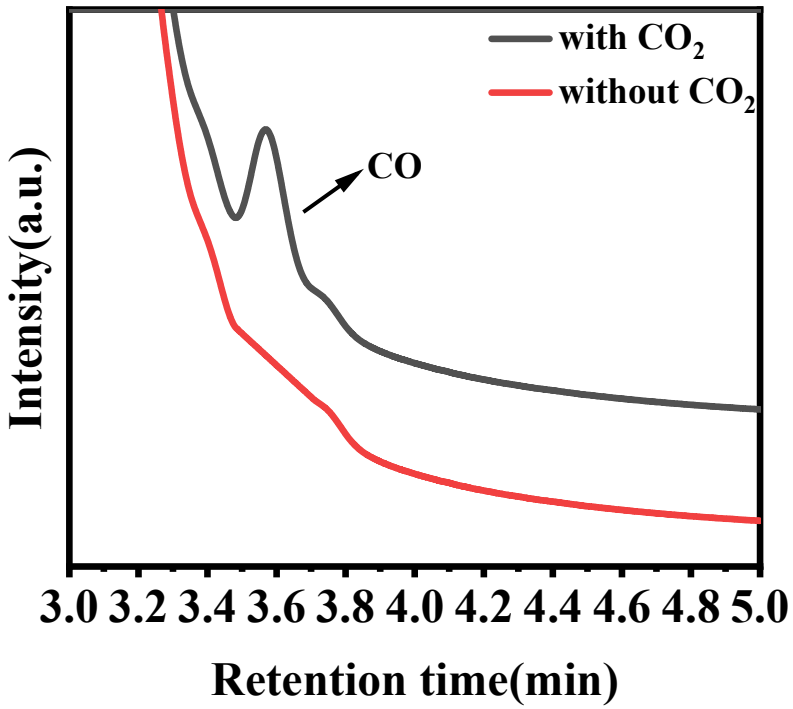

Fig. S31 Control experiment: GC results for CO detection after 10 h of photocatalysis with (black curve) and without (red curve) CO_2.

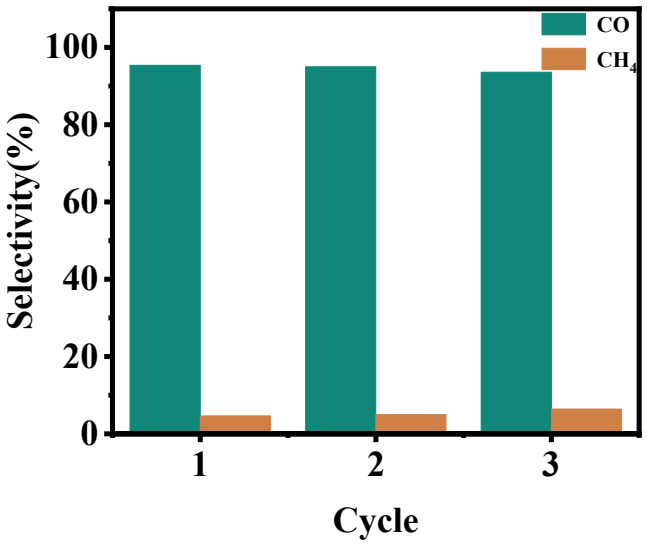

Fig. S32 Selectivity of SUM-33 in three consecutive cycles

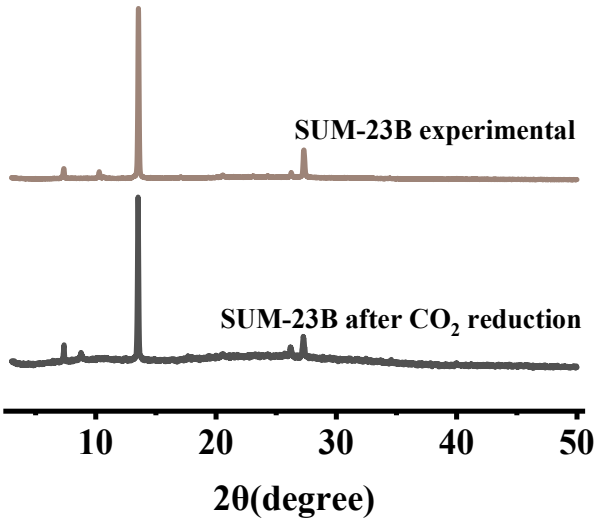

Fig. S33 PXRD of SUM-23B before and after CO2RR.

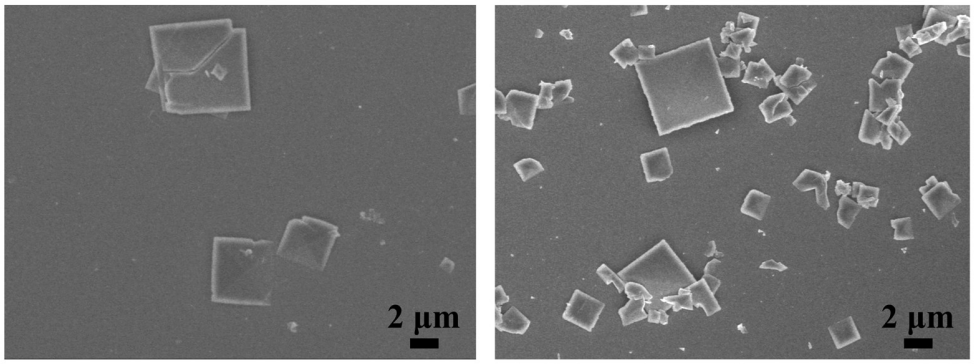

Fig. S34 SEM images of as-synthesized SUM-23B (left) and sample after photocatalytic CO2RR (right).

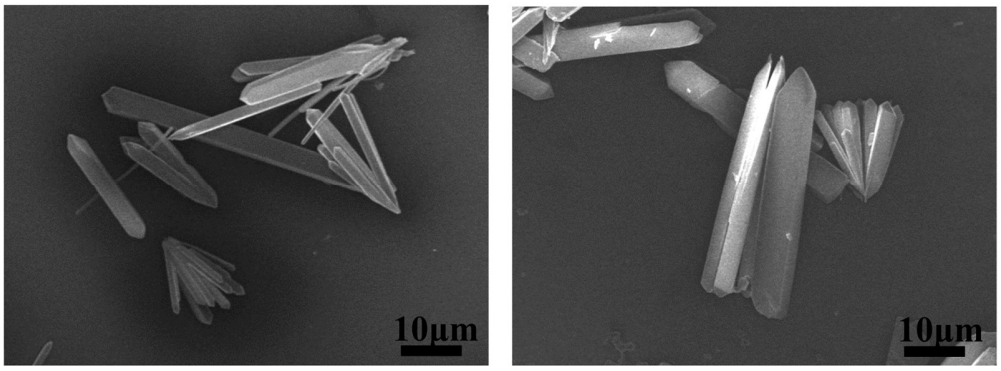

Fig. S35 SEM images of as-synthesized SUM-33 (left) and sample after three consecutive cycles of photocatalytic CO2RR (right).

6. References

1. G. Sheldrick, *Acta Crystallogr. A*, 2008, **64**, 112-122.
2. G. Sheldrick, *Acta Crystallogr. C*, 2015, **71**, 3-8.
3. O. V. Dolomanov, L. J. Bourhis, R. J. Gildea, J. A. K. Howard and H. Puschmann, *J. Appl. Crystallogr.*, 2009, **42**, 339-341.
4. E.-S. M. N. AbdelHafez, O. M. Aly, G. E.-D. A. A. Abuo-Rahma and S. B. King, *Adv. Synth. Catal.*, 2014, **356**, 3456-3464.
5. A. R. Millward and O. M. Yaghi, *J.Am.Chem.Soc.*, 2005, **127**, 17998-17999.
6. Y.-G. Lee, H. R. Moon, Y. E. Cheon and M. P. Suh, *Angew. Chem. Int. Ed.*, 2008, **47**, 7741-7745.
7. A. Demessence, D. M. D'Alessandro, M. L. Foo and J. R. Long, *J.Am.Chem.Soc.*, 2009, **131**, 8784-8786.
8. K. Sumida, S. Horike, S. S. Kaye, Z. R. Herm, W. L. Queen, C. M. Brown, F. Grandjean, G. J. Long, A. Dailly and J. R. Long, *Chem. Sci.*, 2010, **1**, 184-191.
9. L. Hou, W.-J. Shi, Y.-Y. Wang, Y. Guo, C. Jin and Q.-Z. Shi, *ChemComm*, 2011, **47**, 5464-5466.
10. G. Zhang, G. Wei, Z. Liu, S. R. J. Oliver and H. Fei, *Chem. Mater.*, 2016, **28**, 6276-6281.
11. J. Park, D. Yuan, K. T. Pham, J.-R. Li, A. Yakovenko and H.-C. Zhou, *J.Am.Chem.Soc.*, 2012, **134**, 99-102.
12. B. Wang, A. P. Côté, H. Furukawa, M. O'Keeffe and O. M. Yaghi, *Nature*, 2008, **453**, 207-211.
13. Y.-S. Bae, O. K. Farha, A. M. Spokoyny, C. A. Mirkin, J. T. Hupp and R. Q. Snurr, *ChemComm* 2008, DOI: 10.1039/B805785K, 4135-4137.
14. X. Yan, S. Komarneni, Z. Zhang and Z. Yan, *Microporous Mesoporous Mater.*, 2014, **183**, 69-73.
15. X. Feng, Z. Qin, Q. Lai, Z. Zhang, Z.-W. Shao, W. Tang, W. Wu, Z. Dai and C. Liu, *Sep. Purif. Technol.*, 2023, **305**, 122476.
16. E.-X. Chen, M. Qiu, Y.-F. Zhang, Y.-S. Zhu, L.-Y. Liu, Y.-Y. Sun, X. Bu, J. Zhang and Q. Lin, *Adv. Mater.*, 2018, **30**, 1704388.
17. L. Shi, T. Wang, H. Zhang, K. Chang and J. Ye, *Adv. Funct. Mater.*, 2015, **25**, 5360-5367.
18. H. Zhao, X. Wang, J. Feng, Y. Chen, X. Yang, S. Gao and R. Cao, *Catal. Sci. Technol.*, 2018, **8**, 1288-1295.
19. A. Crake, K. C. Christoforidis, A. Kafizas, S. Zafeiratos and C. Petit, *Appl. Catal., B*, 2017, **210**, 131-140.
20. L. Wang, P. Jin, S. Duan, H. She, J. Huang and Q. Wang, *Sci. Bull.*, 2019, **64**, 926-933.
21. L. Wang, P. Jin, J. Huang, H. She and Q. Wang, *ACS Sustainable Chem. Eng.*, 2019, **7**, 15660-15670.
22. N.-Y. Huang, J.-Q. Shen, X.-W. Zhang, P.-Q. Liao, J.-P. Zhang and X.-M. Chen, *J.Am.Chem.Soc.*, 2022, **144**, 8676-8682.
23. J. Lu, S. Wang, Y. Zhao, K. Ge, J. Wang, H. Cui, Y. Yang and Y. Yang, *Catal. Commun.*, 2023, **175**, 106613.
24. Y. Xie, Z. Fang, L. Li, H. Yang and T.-F. Liu, *ACS Appl. Mater. Interfaces*, 2019, **11**, 27017-27023.